

Asymptotical Construction of an Efficient High-Fidelity Model for Multilayer Functionally Graded Plates

Hui Chen* and Wenbin Yu†
Utah State University, Logan, Utah 84322-4130

DOI: 10.2514/1.J050016

An efficient high-fidelity plate model is developed for heterogeneous multilayer laminates made of functionally graded material. Taking advantage of the smallness of the ratio of the thickness to the characteristic wavelength of the deformation of the reference surface, we apply the variational-asymptotic method to rigorously decouple the three-dimensional, anisotropic elasticity problem into a one-dimensional through-the-thickness analysis and a two-dimensional plate analysis. The through-the-thickness analysis provides constitutive relations for the plate analysis as well as the recovery information for the three-dimensional fields, reducing the complex three-dimensional elasticity model to a simple two-dimensional plate model with an excellent tradeoff between efficiency and accuracy. The present model is valid for large displacements and global rotations and can capture all the geometric nonlinearity of a plate when the strains are small. A few examples are used to validate this model.

Nomenclature

\mathbf{B}_i	= base vectors of the coordinate system after deformation	t_1, t_2	= arbitrary fixed times
\mathbf{b}_i	= base vectors of the coordinate system before deformation	U_i	= three-dimensional displacements
C_{ij}	= direction cosine matrix describing the rotation from triad \mathbf{b}_i to triad \mathbf{B}_i	u_i	= two-dimensional displacements
c_{\parallel}	= through-the-thickness average of in-plane warping functions	\mathcal{U}	= three-dimensional strain energy
e_{ijk}	= the permutation symbol	\mathcal{U}_{A0}	= zeroth-order strain energy
F_{ij}	= mixed-basis deformation gradient tensor	\hat{V}_i	= absolute velocity of a material point in three-dimensional configuration
f_i, m_α	= generalized forces and moments, respectively	V_i	= absolute velocity of a point on the deformed reference surface
\mathbf{G}_i	= covariant basis vectors of the deformed configuration	w_i	= warping functions
h	= thickness of the plate	x_i	= Cartesian coordinates
K^*	= effective bulk modulus estimated by the Mori–Tanaka scheme	Γ_{ij}	= three-dimensional strain tensor
\mathcal{K}	= three-dimensional kinetic energy	γ	= transverse shear strains for the Reissner–Mindlin model
\mathcal{K}_{2D}	= two-dimensional kinetic energy	$\overline{\delta\mathcal{W}}$	= three-dimensional virtual work
L_α	= integration constants for determining the relationship between \mathcal{E} and c_{\parallel}	$\overline{\delta\mathcal{W}}_{2D}$	= two-dimensional virtual work
l	= characteristic wavelength of the plate deformation	$\partial\Omega$	= boundary of the reference surface
\mathcal{M}	= plate moment resultants	\mathcal{E}	= column matrix containing two-dimensional generalized strains, $[\varepsilon^T \kappa^T]^T$
\mathcal{N}	= plate force resultants	$\varepsilon_{\alpha\beta}, K_{\alpha\beta}, \varepsilon, \kappa$	= two-dimensional generalized plate strains
Q_i	= tractions applied on lateral surfaces	η	= small parameter used to denote the order of strains
\mathbf{R}	= position vector of a material point on the deformed reference surface	$\lambda_{\parallel}, \lambda_3, \Lambda_3$	= Lagrange multipliers for enforcing in-plane and out-of-plane warping constraints
\mathcal{R}	= generalized strain measures of the Reissner–Mindlin model	μ	= characteristic magnitude of the elastic constants
$\hat{\mathbf{R}}$	= position vector of a material point in the deformed three-dimensional configuration	μ^*	= effective shear modulus estimated by the Mori–Tanaka scheme
\mathbf{r}	= position vector of a material point on the undeformed reference surface	ρ	= mass density
$\hat{\mathbf{r}}$	= position vector of a material point in the undeformed three-dimensional configuration	σ_{ij}	= three-dimensional stress tensor
		τ_i, β_i	= tractions applied on top and bottom surfaces
		ϕ_i	= applied body force
		Ω	= the reference surface
		ω	= inertial angular velocity of triad \mathbf{B}_i

I. Introduction

FUNCTIONALLY graded materials (FGM) have received significant attention in recent years. The various functional effects of FGM have been used to address a large variety of application fields, such as graded thermoelectrics and dielectrics, piezoelectrically graded materials for ultrasonic transducers, and tungsten–copper composites for high-current connectors and diverter plates, to name but a few [1,2]. One extensively investigated FGM, typically used for constructing panels in aerospace systems, is made of a mixture of ceramics and metals and characterized by a continuously changing of its mechanical properties using a smooth change in volume fraction of the constituent materials from one

Received 19 June 2009; revision received 4 November 2009; accepted for publication 6 January 2010. Copyright © 2010 by Hui Chen and Wenbin Yu. Published by the American Institute of Aeronautics and Astronautics, Inc., with permission. Copies of this paper may be made for personal or internal use, on condition that the copier pay the \$10.00 per-copy fee to the Copyright Clearance Center, Inc., 222 Rosewood Drive, Danvers, MA 01923; include the code 0001-1452/10 and \$10.00 in correspondence with the CCC.

*Research Engineer, Department of Mechanical and Aerospace Engineering, Member AIAA.

†Associate Professor, Department of Mechanical and Aerospace Engineering, Senior Lifetime Member AIAA.

surface of the material to the other. The surface with high ceramic constituents can provide superior thermal resistance for high-temperature environments, and the surface with high metal constituents offers strong mechanical performance. This kind of material arrangement reduces the risk of catastrophic fracture under extreme environments. Recently, the concept of FGM is actively explored in the multilayered design of thermal coatings as well as sandwich panels to overcome the mismatch of the thermomechanical properties between the coating and the substrate or between the surface panels and the core [3–6].

To use FGM effectively, we need to develop efficient yet accurate models for structures made of such materials such as FGM plates and shells. These structures are characterized by one of their dimensions (the thickness) being much smaller than the other two. Although all structures made of FGM can be described using three-dimensional (3-D) continuum mechanics, exact solutions exist only for a few specific problems with very idealized material types, geometry, and boundary conditions [4,5,7–9]. For more realistic cases, one often has to rely on 3-D numerical simulation tools such as ANSYS and ABAQUS to find approximate solutions. However, this approach is computation intensive and they are usually used in the detailed analysis due to their prohibitive computational cost. In view of the fact that the thickness is small, analysis of such structures can be simplified using two-dimensional (2-D) models. Although many 2-D models have been developed to analyze FGM plates and shells treating different topics, most of them rely on some a priori kinematic assumptions. Examples may be found in the application of classical lamination theory (CLT) in thermal residual stress and free-vibration analyses [3,10], the use of the first-order shear-deformation theory (FSDT) in active control analysis [11], and the implementation of the third-order shear-deformation theory in bending and buckling analyses [12].

CLT ignores transverse shear effects and provides reasonable results only for very thin plates. Moreover, in CLT, both plane strain and plane stress are assumed, which we know will not be true at the same time for materials having nonzero Poisson's ratios. A number of shear-deformation theories have been developed to overcome some drawbacks of CLT, the simplest of which is FSDT (equivalent to Reissner–Mindlin theory for plates made of isotropic homogeneous materials), in which a constant distribution of shear strain through the thickness is assumed and a shear-correction factor is required to account for the deviation of the real shear strain from the assumed constant one. The dependence of the shear-correction factor on the geometry and material of the plate makes it difficult to guarantee the accuracy of FSDT. By expanding the displacement field of the plate using higher-order polynomials, higher-order shear-deformation plate theories are developed, which can account for both transverse normal and shear deformations without relying on shear-correction factors. However, as indicated by Bian et al. [13] and Das et al. [6] for laminated plates and shells, models based on higher-order theories cannot capture the discontinuous slope of in-plane and transverse displacement components in the thickness direction. By extending a generalized refined theory (referred to as Soldatos plate theory [14,15]) that incorporates shape functions to guarantee continuity of transverse shear stresses at interfaces, these authors provide analytical solutions for simply and multiply spanned functionally graded plates under cylindrical bending [13]. Higher-order shear-deformation theories have also been implemented using the finite element method to analyze functionally graded plates. As recent examples, Gilhooley et al. [16] carried out a numerical investigation of a two-constituent metal/ceramics thick plate by combining a meshless local Petrov–Galerkin method and a higher-order shear-deformation plate theory, and Zhen and Chen [17] combined the higher-order shear-deformation theory with refined three-node triangular element for analyzing multilayered FGMs.

Despite the popularity of the aforementioned methods in analyzing many functionally graded plates and laminated plates, these approaches have two major disadvantages:

1) The a priori assumptions that are naturally extended from the analysis of isotropic homogeneous structures cannot be easily

justified for heterogeneous and anisotropic structures, such as FGMs.

2) It is difficult for an analyst to determine the accuracy of the result and which assumption should be chosen for efficient yet accurate analysis for a particular plate.

Recently, the variational-asymptotic method (VAM) [18] was used to develop a series of rigorous Reissner–Mindlin plate models for heterogeneous and anisotropic composite plates and smart plates [19–25]. These models have excellent compromise between the efficiency and accuracy. In this paper, we expand this method to construct an efficient and high-fidelity model that is able to capture the geometric nonlinearity for multilayer functionally graded plates, for which material properties of each layer can be functions of the thickness coordinate x_3 .

In present work, the 3-D displacement field of an arbitrary material point of the plate is expressed using the deformation of the reference surface along with unknown warping functions, without invoking any a priori kinematic assumptions. The original 3-D elasticity problem is cast in an intrinsic form so that the theory can accommodate arbitrary large deformations and global rotations with the restriction that the strain field is small. Taking advantage of the small parameter h/l , we apply VAM to systematically reduce the original 3-D model to a series of 2-D models, so that the original nonlinear 3-D problem is rigorously split into a linear one-dimensional (1-D) through-the-thickness analysis and a 2-D nonlinear plate analysis. For practical uses, we also transfer the asymptotically correct energy into the Reissner–Mindlin model with the transverse shear stiffness calculated through a least-squares scheme. To validate this model, we analyzed a couple of examples, and excellent agreement with the 3-D exact elasticity solution has been achieved using the present model.

II. Three-Dimensional Formulation

The elastodynamic behavior of a solid is governed by the extended Hamilton principle:

$$\int_{t_1}^{t_2} [\delta(\mathcal{K} - \mathcal{U}) + \overline{\delta\mathcal{W}}] dt = 0 \quad (1)$$

where the overbar is used to indicate that the virtual work $\overline{\delta\mathcal{W}}$ does not necessarily represent variation of a function; in other words, there may not exist such a functional \mathcal{W} that its variation is equal to the virtual work done by the applied loads.

A point in the plate can be described by its Cartesian coordinates x_i (see Fig. 1), in which x_α are two orthogonal lines in the reference surface and x_3 is the normal coordinate originating from the middle of the thickness. Throughout the analysis, Greek indices assume values 1 and 2, and Latin indices assume 1, 2, and 3; repeated indices are summed over their range, except that they are explicitly indicated.

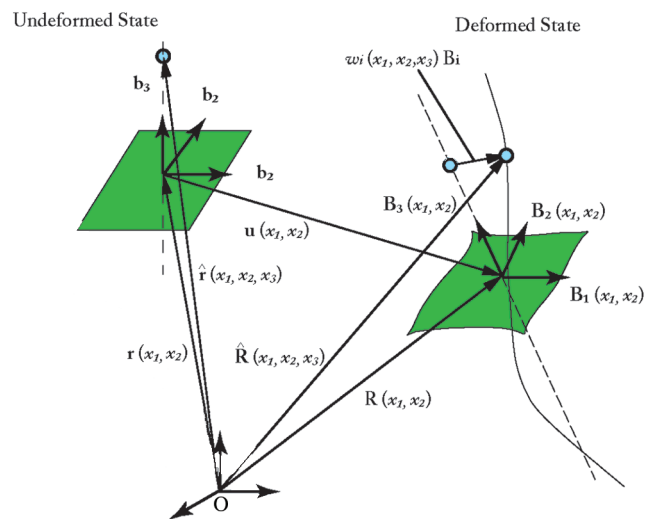


Fig. 1 Schematic of plate deformation.

Letting \mathbf{b}_i denote the unit vector along x_i for the undeformed plate, we can then describe the position of any material point in the undeformed configuration by its position vector $\hat{\mathbf{r}}$ from a fixed point O , such that

$$\hat{\mathbf{r}}(x_1, x_2, x_3, t) = \mathbf{r}(x_1, x_2, t) + x_3 \mathbf{b}_3 \quad (2)$$

where \mathbf{r} is the position vector from a fixed point O to the point located by x_a on the reference surface at a specific time t . When the reference surface of the undeformed plate coincides with its middle surface, we have

$$\langle \hat{\mathbf{r}}(x_1, x_2, x_3, t) \rangle = h\mathbf{r}(x_1, x_2, t) \quad (3)$$

where the angle bracket denotes the definite integral through the thickness of the plate.

When the plate deforms, the particle that had position vector $\hat{\mathbf{r}}$ in the undeformed state now has position vector $\hat{\mathbf{R}}$ in the deformed plate, which can be uniquely determined by the deformation of the 3-D body. We introduce another orthonormal triad \mathbf{B}_i for the deformed configuration so that

$$\mathbf{B}_i = C_{ij} \mathbf{b}_j, \quad C_{ij} = \mathbf{B}_i \cdot \mathbf{b}_j \quad (4)$$

subjecting to the requirement that \mathbf{B}_i is coincident with \mathbf{b}_i when the structure is undeformed. The direction cosines matrix $C(x_1, x_2)$ represents the possible arbitrary rotation between \mathbf{B}_i and \mathbf{b}_i .

After deformation, the position vector $\hat{\mathbf{R}}$ in the deformed state can be expressed as

$$\begin{aligned} \hat{\mathbf{R}}(x_1, x_2, x_3, t) &= \mathbf{R}(x_1, x_2, t) + x_3 \mathbf{B}_3(x_1, x_2, t) \\ &+ w_i(x_1, x_2, x_3, t) \mathbf{B}_i(x_1, x_2, t) \end{aligned} \quad (5)$$

where \mathbf{R} is the position vector of the reference surface for the deformed plate and $w_i(x_1, x_2, x_3, t)$ are the warping functions introduced to accommodate all possible deformations. Equation (5) can be considered as a change of variables for $\hat{\mathbf{R}}$ in terms of \mathbf{R} , \mathbf{B}_i , and w_i . Proper definitions of \mathbf{R} and \mathbf{B}_i are needed to introduce six constraints to ensure a one-to-one mapping of this change of variables. We can introduce the following three constraints for the warping functions:

$$\langle w_i(x_1, x_2, x_3, t) \rangle = \begin{Bmatrix} c_{\parallel} \\ 0 \end{Bmatrix}, \quad \text{with} \quad c_{\parallel} = \begin{Bmatrix} c_1 \\ c_2 \end{Bmatrix} \quad (6)$$

where c_1 and c_2 are functions of the in-plane coordinates x_a and time t , introduced for providing free variables for the construction of an optimal Reissner–Mindlin model, which will be described later. Two other constraints can be specified by taking \mathbf{B}_3 as the normal to the reference surface of the deformed plate. It should be noted that this choice has nothing to do with the well-known Kirchhoff hypothesis. In the Kirchhoff assumption, no local deformation of the transverse normal is allowed. However, in present derivation we allow all possible deformation using the warping functions. Because \mathbf{B}_α can freely rotate around \mathbf{B}_3 , we can introduce the last constraint as

$$\mathbf{B}_1 \cdot \mathbf{R}_{,2} = \mathbf{B}_2 \cdot \mathbf{R}_{,1} \quad (7)$$

where comma denotes a partial derivative so that $f_{,a} = \partial f / \partial x_a$.

Based on the concept of decomposition of rotation tensor [26,27], the Jauman–Biot–Cauchy strain components for small local rotation are given by

$$\Gamma_{ij} = \frac{1}{2}(F_{ij} + F_{ji}) - \delta_{ij} \quad (8)$$

with

$$F_{ij} = \mathbf{B}_i \cdot \mathbf{G}_k \mathbf{b}_k \cdot \mathbf{b}_j \quad (9)$$

Here, $\mathbf{G}_k = \partial \hat{\mathbf{R}} / \partial x_k$ is the covariant basis vector of the deformed configuration. The details for obtaining this concise expression for the Jauman–Biot–Cauchy strain tensor can be found in [26]. To

express the 3-D strain field in terms of 2-D plate strains, we can define the 2-D generalized strains following [28] as

$$\mathbf{R}_{,\alpha} = \mathbf{B}_\alpha + \varepsilon_{\alpha\beta} \mathbf{B}_\beta \quad (10)$$

$$\mathbf{B}_{i,\alpha} = (-K_{\alpha\beta} \mathbf{B}_\beta \times \mathbf{B}_3 + K_{\alpha 3} \mathbf{B}_3) \times \mathbf{B}_i \quad (11)$$

Using this definition, one can show that Eq. (7) implies $\varepsilon_{12} = \varepsilon_{21}$. The expressions for 2-D generalized strained in terms of plate displacements and rotations can be found in [28].

For geometrically nonlinear analysis, we can assume that both the 3-D and 2-D strains are small when compared with the unity and from that we can also conclude that warpings are of the order of the strain or smaller. Using Eq. (8) along with Eqs. (2), (5), and (9–11), we can derive the following expression for the 3-D strain field:

$$\begin{aligned} \Gamma_e &= \varepsilon + x_3 \kappa + I_1 w_{\parallel,1} + I_2 w_{\parallel,2} \\ 2\Gamma_s &= w'_1 + e_1 w_{3,1} + e_2 w_{3,2} \quad \Gamma_t = w'_3 \end{aligned} \quad (12)$$

where prime denotes $\partial(\cdot) / \partial x_3$, \parallel values denote $[\cdot]_1 \quad [\cdot]_2]^T$, and

$$\begin{aligned} \Gamma_e &= [\Gamma_{11} \quad 2\Gamma_{12} \quad \Gamma_{22}]^T, \quad 2\Gamma_s = [2\Gamma_{13} \quad 2\Gamma_{23}]^T, \quad \Gamma_t = \Gamma_{33} \\ \varepsilon &= [\varepsilon_{11} \quad 2\varepsilon_{12} \quad \varepsilon_{22}]^T, \quad \kappa = [K_{11} \quad K_{12} + K_{21} \quad K_{22}]^T \end{aligned} \quad (13)$$

$$I_1 = \begin{Bmatrix} 1 & 0 \\ 0 & 1 \\ 0 & 0 \end{Bmatrix}, \quad I_2 = \begin{Bmatrix} 0 & 0 \\ 1 & 0 \\ 0 & 1 \end{Bmatrix}, \quad e_1 = \begin{Bmatrix} 1 \\ 0 \end{Bmatrix}, \quad e_2 = \begin{Bmatrix} 0 \\ 1 \end{Bmatrix} \quad (14)$$

Note that in deriving Eq. (12), we have neglected the products between warping and strain because these terms are negligible based on our small strain assumption. With the knowledge of the 3-D strain field, we can express the strain energy as

$$\begin{aligned} U &= \int_{\Omega} \frac{1}{2} \left\langle \begin{Bmatrix} \Gamma_e \\ 2\Gamma_s \\ \Gamma_t \end{Bmatrix}^T \begin{bmatrix} C_e & C_{es} & C_{et} \\ C_{es}^T & C_s & C_{st} \\ C_{et}^T & C_{st}^T & C_t \end{bmatrix} \begin{Bmatrix} \Gamma_e \\ 2\Gamma_s \\ \Gamma_t \end{Bmatrix} \right\rangle d\Omega \\ &\equiv \int_{\Omega} \mathcal{U}_A d\Omega \end{aligned} \quad (15)$$

where C_e , C_{es} , C_{et} , C_s , C_{st} , and C_t are the corresponding partition matrices of the 3-D 6×6 material matrix, which are functions of x_i for functionally graded materials. Here, for simplicity, we restrict ourselves to FGM plates having material properties as functions of x_3 only.

To calculate the kinetic energy, the absolute velocity of a generic point in the structure is obtained by taking a time derivative of Eq. (5) as

$$\hat{\mathbf{V}} = \mathbf{V} + \tilde{\omega}(\xi + w) + \dot{w} \quad (16)$$

where the dot is the partial derivative with respect to time and the tilde notation forms an antisymmetric matrix from a vector according to $\tilde{O}_{ij} = -e_{ijk}(\cdot)_k$. In Eq. (16), the symbols $\hat{\mathbf{V}}$, \mathbf{V} , and ω denote column matrices containing the components of corresponding vectors in \mathbf{B}_i bases, and $\xi = [0 \quad 0 \quad x_3]^T$. The kinetic energy of the plate structure can be obtained by

$$\mathcal{K} = \frac{1}{2} \int_V \rho \hat{\mathbf{V}}^T \hat{\mathbf{V}} dV = \mathcal{K}_{2D} + \mathcal{K}^* \quad (17)$$

with

$$\mathcal{K}_{2D} = \frac{1}{2} \int_{\Omega} (\bar{\mu} V^T V + 2\omega^T \mu \tilde{\xi} V + \omega^T j \omega) d\Omega \quad (18)$$

$$\mathcal{K}^* = \frac{1}{2} \int_V \rho [(\tilde{\omega}w + \dot{w})^T (\tilde{\omega}w + \dot{w}) + 2(V + \tilde{\omega}\xi)^T (\tilde{\omega}w + \dot{w})] dV \quad (19)$$

where $\bar{\mu}$, $\mu\bar{\xi}$, and j are inertial constants commonly used in plate dynamics, which can be trivially obtained by taking integral operations through the thickness:

$$\bar{\mu} = \langle \rho \rangle, \quad \mu\bar{\xi} = [0 \quad 0 \quad \langle x_3 \rho \rangle]^T, \quad j = \begin{bmatrix} \langle x_3^2 \rho \rangle & 0 & 0 \\ 0 & \langle x_3^2 \rho \rangle & 0 \\ 0 & 0 & 0 \end{bmatrix} \quad (20)$$

The virtual work of the structure can be calculated as

$$\overline{\delta\mathcal{W}} = \int_{\Omega} ((\phi \cdot \delta\hat{\mathbf{R}}) + \tau \cdot \delta\hat{\mathbf{R}}^+ + \beta \cdot \delta\hat{\mathbf{R}}^-) d\Omega + \int_{\partial\Omega} \langle \mathbf{Q} \cdot \delta\hat{\mathbf{R}} \rangle ds \quad (21)$$

where superscripts $+$ or $-$ denote $(\cdot)|_{x_3=\pm h/2}$; $\phi = \phi_i \mathbf{B}_i$ is the applied body force; $\tau = \tau_i \mathbf{B}_i$ and $\beta = \beta_i \mathbf{B}_i$ are tractions applied on the top and bottom surfaces, respectively; $\mathbf{Q} = Q_i \mathbf{B}_i$ are the applied tractions along the lateral surfaces; and $\delta\hat{\mathbf{R}}$ is the Lagrangian variation of the displacement field, which can be expressed as

$$\delta\hat{\mathbf{R}} = \overline{\delta q}_i \mathbf{B}_i + x_3 \delta \mathbf{B}_3 + \delta w_i \mathbf{B}_i + w_j \delta \mathbf{B}_j \quad (22)$$

where the virtual displacement and rotation are defined by

$$\overline{\delta q}_i = \delta \mathbf{R} \cdot \mathbf{B}_i, \quad \delta \mathbf{B}_i = (-\overline{\delta \psi}_2 \mathbf{B}_1 + \overline{\delta \psi}_1 \mathbf{B}_2 + \overline{\delta \psi}_3 \mathbf{B}_3) \times \mathbf{B}_i \quad (23)$$

where $\overline{\delta q}_i$ and $\overline{\delta \psi}_i$ contain the components of the virtual displacement and rotation in the \mathbf{B}_i system, respectively. Since the warping functions are small, one may safely ignore products of the warping functions and the virtual rotations in $\delta\hat{\mathbf{R}}$ and obtain the virtual work due to applied loads as

$$\overline{\delta\mathcal{W}} = \overline{\delta\mathcal{W}}_{2D} + \overline{\delta\mathcal{W}}^*, \quad (24)$$

where

$$\begin{aligned} \overline{\delta\mathcal{W}}_{2D} &= \int_{\Omega} (f_i \overline{\delta q}_i + m_{\alpha} \overline{\delta \psi}_{\alpha}) d\Omega \\ &+ \int_{\partial\Omega} ((Q_i) \overline{\delta q}_i + \langle x_3 Q_{\alpha} \rangle \overline{\delta \psi}_{\alpha}) ds \end{aligned} \quad (25)$$

$$\overline{\delta\mathcal{W}}^* = \int_{\Omega} ((\phi_i \delta w_i) + \tau_i \delta w_i^+ + \beta_i \delta w_i^-) d\Omega + \int_{\partial\Omega} \langle Q_i \delta w_i \rangle ds \quad (26)$$

with the generalized forces f_i and moments m_{α} defined as

$$f_i = \langle \phi_i \rangle + \tau_i + \beta_i, \quad m_{\alpha} = \langle x_3 \phi_{\alpha} \rangle + \frac{h}{2} (\tau_{\alpha} - \beta_{\alpha}) \quad (27)$$

The second integration in Eq. (26) accounts for the virtual work done through warping functions along the lateral boundaries of the plate. This term is necessary for the edge-zone problem, which is an important subject in its own right and beyond the scope of the present paper. For simplicity, we will drop this term hereafter. With the knowledge of Eqs. (15), (17), and (24), the extended Hamilton's principle in Eq. (1) becomes

$$\int_{t_1}^{t_2} [\delta(\mathcal{K}_{2D} + \mathcal{K}^* - \mathcal{U}) + \overline{\delta\mathcal{W}}_{2D} + \overline{\delta\mathcal{W}}^*] dt = 0 \quad (28)$$

So far, we have presented a 3-D formulation for the plate structure in terms of 2-D displacements (represented by $\mathbf{R} - \mathbf{r}$), 2-D rotations (represented by \mathbf{b}_i and \mathbf{B}_i), and 3-D warping functions w_i . If we attempt to solve this problem directly, we will meet the same

difficulty as solving any full 3-D problem with the additional difficulty coming from the anisotropy and heterogeneity of functionally graded materials. The main complexity comes from the unknown 3-D warping functions w_i . A common practice in the literature is to use a priori assumptions. However, for plates made with general anisotropic and heterogeneous materials such as functionally graded materials, imposition of such assumptions may introduce significant errors. Fortunately, VAM provides a useful technique to obtain w_i through an asymptotical analysis of the variational statement in Eq. (28) in terms of small parameters inherent in the problem that will be described in the next section.

III. Dimensional Reduction

The dimensional reduction from the original 3-D formulation to a 2-D plate model can only be done approximately. One way to accomplish this is to take advantage of the small parameters in the formulation to construct a 2-D formulation so that the loss of accuracy can be minimized.

To apply VAM, we first need to assess the order of quantities in terms of small parameters. As mentioned previously, the ratio of the plate thickness to the characteristic wavelength of the deformation of the reference surface is small, $h/l \ll 1$. The strain is also small if we are only interested in a geometrically nonlinear but physically linear 2-D theory: $\epsilon_{\alpha\beta} \sim h\kappa_{\alpha\beta} \sim \eta \ll 1$. From the plate equations of equilibrium, we can estimate the orders of the following quantities corresponding to the order of strains:

$$\begin{aligned} h\phi_3 \sim \tau_3 \sim \beta_3 \sim \mu(h/l)^2 \eta, \quad h\phi_{\alpha} \sim \tau_{\alpha} \sim \beta_{\alpha} \sim \mu(h/l) \eta \\ Q_{\alpha} \sim \mu \eta, \quad Q_3 \sim \mu(h/l) \eta \end{aligned} \quad (29)$$

We can choose the characteristic scale of change of the displacements and warping functions with respect to time in such a way that \mathcal{K}^* is much smaller than other terms in Eq. (28). In other words, here we are only interested in the accurate description of low-frequency dynamic problems.

A. Zeroth-Order Approximation

To clearly illustrate the application of VAM for FGM plates, we first construct a classical FGM plate model. By applying VAM, the zeroth-order approximation of the variational statement in Eq. (28) can be obtained as

$$\int_{t_1}^{t_2} [\delta(\mathcal{K}_{2D} - \int_{\Omega} \mathcal{U}_{A0} d\Omega) + \overline{\delta\mathcal{W}}_{2D}] dt = 0 \quad (30)$$

where \mathcal{U}_{A0} can be obtained from Eq. (15) by dropping the derivatives with respect to x_{α} in Eq. (12), resulting in

$$\begin{aligned} 2\mathcal{U}_{A0} &= 2\langle (\epsilon + x_3 \kappa)^T (C_{es} w'_{\parallel} + C_{et} w'_3) + w'_{\parallel} C_{st} w'_3 \rangle \\ &+ \langle (\epsilon + x_3 \kappa)^T C_e (\epsilon + x_3 \kappa) + w'_{\parallel} C_s w'_{\parallel} + w'_3 C_t w'_3 \rangle \\ &+ o\left(\left(\frac{h}{l}\right)^0 \eta^2\right) \end{aligned} \quad (31)$$

It is obvious that the warping functions w_i can be obtained by solving the following variational statement,

$$\delta\mathcal{U}_{A0} = 0 \quad (32)$$

along with the constraint equation expressed in Eq. (6). The corresponding Euler-Lagrange equations are

$$\begin{aligned} [(\epsilon + x_3 \kappa)^T C_{et}^{(k)} + w'_{\parallel}{}^{(k)T} C_{st}^{(k)} + w'_3{}^{(k)} C_t^{(k)}] \gamma &= \lambda_3, \\ [(\epsilon + x_3 \kappa)^T C_{es}^{(k)} + w'_{\parallel}{}^{(k)T} C_s^{(k)} + w'_3{}^{(k)} C_{st}^{(k)T}] &= \lambda_{\parallel}, \end{aligned} \quad (33)$$

$k = 1, 2, 3, \dots, N$

where λ_{\parallel} and λ_3 are Lagrange multipliers corresponding to the in-plane and out-of-plane constraint equations expressed in Eq. (6); γ denotes functions for the k th layer. The boundary conditions as well as the interlaminar continuous conditions are

$$\begin{aligned} [(\epsilon + x_3\kappa)^T C_{et} + w_{\parallel}^T C_{st} + w_3' C_t]^+ &= 0 \\ [(\epsilon + x_3\kappa)^T C_{es} + w_{\parallel}^T C_s + w_3' C_{st}^-]^- &= 0 \end{aligned} \quad (34)$$

and

$$\begin{aligned} [w_3] &= 0, & [(\epsilon + x_3\kappa)^T C_{et} + w_{\parallel}^T C_{st} + w_3' C_t] &= 0, & \text{on } \Omega_i \\ [w_{\parallel}] &= 0, & [(\epsilon + x_3\kappa)^T C_{es} + w_{\parallel}^T C_s + w_3' C_{st}^-] &= 0, & \text{on } \Omega_i \end{aligned} \quad (35)$$

respectively. Here, Ω_i denotes the interfaces between the i th layer and $i + 1$ th layer; $i = 1, \dots, N - 1$, with N denoting the total number of layers; the brackets denote the jump of the enclosed argument on the interface. From these conditions, we can solve w_i' from Eq. (33),

$$w_{\parallel}^{(k)T} = -(\epsilon + x_3\kappa)^T \hat{C}_{es}^{(k)} C_s^{(k)-1}, \quad w_3^{(k)} = -(\epsilon + x_3\kappa)^T \hat{C}_{et}^{(k)} / \hat{C}_t^{(k)} \quad (36)$$

with the hatted quantities being expressed as

$$\begin{aligned} \hat{C}_{es}^{(k)} &= C_{es}^{(k)} - \hat{C}_{et}^{(k)} C_{st}^{(k)T} / C_t^{(k)} \\ \hat{C}_{et}^{(k)} &= C_{et}^{(k)} - C_{es}^{(k)} C_s^{(k)-1} C_{st}^{(k)} \\ \hat{C}_t^{(k)} &= C_t^{(k)} - C_{st}^{(k)T} C_s^{(k)-1} C_{st}^{(k)} \end{aligned} \quad (37)$$

Substituting Eq. (36) into Eq. (31), we obtain the zeroth-order strain energy as

$$2\mathcal{U}_{A0} = \begin{Bmatrix} \epsilon \\ \kappa \end{Bmatrix}^T \begin{bmatrix} \hat{A} & \hat{B} \\ \hat{B}^T & \hat{D} \end{bmatrix} \begin{Bmatrix} \epsilon \\ \kappa \end{Bmatrix} + o\left(\left(\frac{h}{l}\right)^0 \eta^2\right) \quad (38)$$

with

$$\begin{aligned} \hat{A} &= \langle \hat{C}_e \rangle, & \hat{B} &= \langle x_3 \hat{C}_e \rangle, & \hat{D} &= \langle x_3^2 \hat{C}_e \rangle \\ \hat{C}_e &= C_e - C_{es} C_s^{-1} \hat{C}_{es}^T - C_{et} \hat{C}_{et}^T / \hat{C}_t \end{aligned} \quad (39)$$

With \mathcal{U}_{A0} expressed in Eq. (38), the original 3-D problem in Eq. (1) has been rigorously reduced to a 2-D formulation in Eq. (30), which approximates the original problem asymptotically correct to the order of $(h/l)^0$. If we define the force resultants \mathcal{N} and moment resultants \mathcal{M} by

$$\mathcal{N} = \frac{\partial \mathcal{U}_{A0}}{\partial \epsilon}, \quad \mathcal{M} = \frac{\partial \mathcal{U}_{A0}}{\partial \kappa} \quad (40)$$

we obtain a 2-D constitutive model for the classical plate analysis of FGM plates, expressed as

$$\begin{Bmatrix} \mathcal{N} \\ \mathcal{M} \end{Bmatrix} = \begin{bmatrix} \hat{A} & \hat{B} \\ \hat{B}^T & \hat{D} \end{bmatrix} \begin{Bmatrix} \epsilon \\ \kappa \end{Bmatrix} \quad (41)$$

It is clear that although the plate is made of functionally gradient materials, the 2-D plate model of the zeroth-order remains the same as CLT. Despite the similarity with CLT, the present model is asymptotically correct and has the following features in contrast with CLT:

1) The normal line of undeformed plate does not remain straight and normal to the deformed plate; rather, it deforms in both the normal and in-plane directions in response to plate deformation (ϵ and κ).

2) This model can handle general functionally gradient materials with full anisotropy.

3) It can be easily observed that neither the normal strain nor the transverse shear strains vanish. The transverse normal and shear stresses can be shown to vanish, which are not assumed a priori but can be concluded from the derivation. It is worth emphasizing that no a priori assumptions, such as setting the transverse normal strain equal to zero, were used in the derivation.

For the zeroth-order approximation, the 3-D strain field can be recovered using Eqs. (12) by neglecting those terms of order higher than $(h/l)^0$:

$$\Gamma_e^0 = \epsilon + x_3\kappa, \quad 2\Gamma_s^0 = w_{\parallel}', \quad \Gamma_t^0 = w_3' \quad (42)$$

Up to this point, the zeroth-order solution w_i in Eq. (36) as well as the 2-D strain energy in Eq. (38) are valid for FGM plates with fully populated 6×6 material matrix C . As most real materials have at least a monoclinic symmetry about their own midplane, hereafter, monoclinic material matrix characterized by 13 independent material properties, implying $C_{es} = 0$ and $C_{st} = 0$, will be used for the rest of derivation. This leads to much simpler expressions for the zeroth-order approximation of warping function:

$$w_{\parallel}^{(k)} = 0, \quad w_3^{(k)} = C_{\perp}^{(k)} \mathcal{E}, \quad k = 1, 2, 3, \dots, N \quad (43)$$

where

$$C_{\perp}^{(k)} = [-C_{et}^{(k)T} / C_t^{(k)} - x_3 C_{es}^{(k)T} / C_t^{(k)}], \quad \mathcal{E} = [\epsilon \ \kappa]^T, \quad \langle C_{\perp} \rangle = 0 \quad (44)$$

Note that interlamina continuity of $C_{\perp}^{(k)}$ must be maintained due to the continuity of warping functions to produce a continuous displacement field. It should also be pointed out that we have constrained in-plane warpings to vanish ($w_{\parallel} = 0$), as the free constants in Eq. (6) will be absorbed in the first-order approximation.

B. First-Order Approximation

To obtain the first-order approximation, we simply perturb the zeroth-order warping functions as

$$w_{\parallel} = v_{\parallel} + o\left(\frac{h}{l}\eta\right), \quad w_3 = v_3 + C_{\perp} \mathcal{E} + o\left(\frac{h}{l}\eta\right) \quad (45)$$

Substituting Eq. (45) back into Eq. (12), and using Eqs. (15), (24), (26), and (28), one can obtain the leading terms for the first-order approximation of the variational statement in Eq. (28) as

$$\begin{aligned} \delta \Pi_1^* &= \langle v_{\parallel}^T C_s \delta v_{\parallel}' + v_3' C_t \delta v_3' + (\epsilon + x_3\kappa)^T C_{\parallel} I_{\alpha} \delta v_{\parallel, \alpha} \\ &+ (e_{\alpha} C_{\perp} \mathcal{E}_{, \alpha})^T C_s \delta v_{\parallel}' - \phi_{\parallel}^T \delta v_{\parallel} \rangle - \tau_{\parallel}^T \delta v_{\parallel}' \\ &- \beta_{\parallel}^T \delta v_{\parallel} + o\left(\left(\frac{h}{l}\right)^2 \eta^2\right) \end{aligned} \quad (46)$$

where $C_{\parallel} = C_e - C_{et} C_{et}^T / C_t$.

It can be easily observed that v_3 is decoupled from v_{\parallel} . Considering the warping constraint in Eq. (6), v_3 only has a trivial solution. The stationary conditions of the functional given in Eq. (46) are

$$\begin{aligned} (C_s^{(k)} v_{\parallel}' + C_s^{(k)} e_{\alpha} C_{\perp}^{(k)} \mathcal{E}_{, \alpha})' &= D_{\alpha}^{(k)} \mathcal{E}_{, \alpha} + g^{(k)} + \lambda_{\parallel} \\ (C_s v_{\parallel}' + C_s e_{\alpha} C_{\perp} \mathcal{E}_{, \alpha})^+ &= \tau_{\parallel} \quad (C_s v_{\parallel}' + C_s e_{\alpha} C_{\perp} \mathcal{E}_{, \alpha})^- = -\beta_{\parallel} \end{aligned} \quad (47)$$

where $D_{\alpha}^{(k)} = -I_{\alpha}^T [C_{\parallel}^{(k)} \ x_3 C_{\parallel}^{(k)}]$, $g^{(k)} = -\phi_{\parallel}^{(k)}$, and λ_{\parallel} are Lagrange multipliers to enforce the constraints in Eq. (6). The continuity conditions on the interfaces can be derived as

$$[v_{\parallel}] = 0, \quad [C_s (v_{\parallel}' + e_{\alpha} C_{\perp} \mathcal{E}_{, \alpha})] = 0 \quad \text{on } \Omega_i \quad (48)$$

The interlamina continuity on $D_{\alpha}^{(k)}$ and $g^{(k)}$ are maintained by the second condition in Eq. (48). It should be mentioned that since the goal is to obtain an interior solution for the plate without considering edge effects, integration by parts with respect to the in-plane coordinates is used hereafter and throughout the rest of the paper, whenever it is convenient for the derivation.

Integrating the first equation in Eq. (47), one obtains

$$C_s^{(k)} v_{\parallel} + C_s^{(k)} e_{\alpha} C_{\perp}^{(k)} \mathcal{E}_{, \alpha} = D_{\alpha}^{(k)} \mathcal{E}_{, \alpha} + g^{(k)} + \lambda_{\parallel} x_3 + \text{const}_{\parallel}^{(k)} \quad (49)$$

and the interface continuity condition in the second equation of Eq. (48) becomes

$$\text{const}_{\parallel}^{(k+1)} - \text{const}_{\parallel}^{(k)} = D_{\alpha}^{(k)}(z_{k+1})\mathcal{E}_{,\alpha} + g^{(k)}(z_{k+1}) \quad (50)$$

where $\text{const}_{\parallel}^{(k)}$ is the integration constant for k th layer, z_k is the x_3 coordinate of the bottom of the k th layer, and $D_{\alpha}^{(k)}$ and $g_{\alpha}^{(k)}$ are defined as

$$D_{\alpha}^{(k)}(x_3) = \int_{z_k}^{x_3} D_{\alpha}^{\prime(k)} dz = - \int_{z_k}^{x_3} I_{\alpha}^T [C_{\parallel}^{(k)} \quad zC_{\parallel}^{(k)}] dz \quad (51)$$

$$g_{\alpha}^{(k)}(x_3) = \int_{z_k}^{x_3} g_{\alpha}^{\prime(k)} dz = - \int_{z_k}^{x_3} \phi_{\parallel}^{(k)} dz \quad (52)$$

Solving Eqs. (49) and (50), the two boundary equations in Eq. (47) as well as Eq. (6), one obtains the following Lagrange multipliers and warping functions:

$$\lambda_{\parallel} = \frac{1}{h}(\tau_{\parallel} + \beta_{\parallel} - \langle D_{\alpha}^{\prime} \rangle \mathcal{E}_{,\alpha} - \langle g^{\prime} \rangle) \quad (53)$$

$$v_{\parallel}^{(k)} = (\bar{D}_{\alpha}^{(k)} + L_{\alpha})\mathcal{E}_{,\alpha} + \bar{g}^{(k)} \quad (54)$$

with

$$\begin{aligned} \bar{D}_{\alpha}^{(k)\prime} &= C_s^{(k-1)} D_{\alpha}^{(k)*}, & \langle \bar{D}_{\alpha} \rangle &= 0, & \bar{g}^{(k)} &= C_s^{(k-1)} g^{(k)*} \\ \langle \bar{g} \rangle &= 0, & L_{\alpha} \mathcal{E}_{,\alpha} &= c_{\parallel}/h \end{aligned} \quad (55)$$

where $D_{\alpha}^{(k)*}$ and $g^{(k)*}$ can be obtained from Eqs. (49), (50), and (53) as well as the boundary conditions in Eq. (47).

Now we are ready to obtain an expression for the total energy that is asymptotically correct through the order of $\mu(h/l)^2\eta^2$, viz.,

$$\begin{aligned} 2\Pi_1 &= \mathcal{E}^T A \mathcal{E} + \mathcal{E}_{,1}^T B \mathcal{E}_{,1} + 2\mathcal{E}_{,1}^T C \mathcal{E}_{,2} + \mathcal{E}_{,2}^T D \mathcal{E}_{,2} \\ &\quad - 2\mathcal{E}^T F + o\left(\left(\frac{h}{l}\right)^2 \eta^2\right) \end{aligned} \quad (56)$$

where

$$\begin{aligned} A &= \begin{bmatrix} \langle C_{\parallel} \rangle & \langle x_3 C_{\parallel} \rangle \\ \langle x_3 C_{\parallel} \rangle & \langle x_3^2 C_{\parallel} \rangle \end{bmatrix} \\ B &= \langle C_{s_{11}} C_{\perp}^T C_{\perp} - D_1^{*T} C_s^{-1} D_1^* \rangle + L_1^T \langle D_1 \rangle + \langle D_1 \rangle^T L_1 \\ C &= \langle C_{s_{12}} C_{\perp}^T C_{\perp} - D_1^{*T} C_s^{-1} D_2^* \rangle + L_1^T \langle D_2 \rangle + \langle D_1 \rangle^T \\ D &= \langle C_{s_{22}} C_{\perp}^T C_{\perp} - D_2^{*T} C_s^{-1} D_2^* \rangle + L_2^T \langle D_2 \rangle + \langle D_2 \rangle^T \\ F &= C_{\perp}^{+T} \tau_3 + C_{\perp}^{-T} \beta_3 + \langle C_{\perp}^T \phi_3 \rangle - \langle D_{\alpha}^{*T} C_s^{-1} g_{\alpha}^* \rangle \\ &\quad - L_{\alpha}^T (\tau_{\parallel} + \beta_{\parallel} + \langle \phi_{\parallel} \rangle)_{,\alpha} \end{aligned} \quad (57)$$

Equation (56) is an energy functional expressed in terms of 2-D variables that can asymptotically approximate the original 3-D energy. It is noted that quadratic terms of the applied loads are neglected, as they will not affect the 2-D model.

IV. Transforming into the Reissner–Mindlin Model

Although Eq. (56) is asymptotically correct through the second order and straightforward use of this strain energy is possible, it involves more complex boundary conditions than necessary, since it contains derivatives of the generalized strain measures. To obtain an energy functional that is of practical use, one can transform Eq. (56) into the Reissner–Mindlin model. In the Reissner–Mindlin model, there are two additional degrees of freedom, which are the transverse shear strains incorporated into the rotation of transverse normal. We introduce another triad \mathbf{B}_i^* for the deformed plate, so that the definition of 2-D strains becomes

$$\begin{aligned} \mathbf{R}_{,\alpha} &= \mathbf{B}_{\alpha}^* + \varepsilon_{\alpha\beta}^* \mathbf{B}_{\beta}^* + 2\gamma_{\alpha 3}^* \mathbf{B}_3^* \\ \mathbf{B}_{i,\alpha}^* &= (-K_{\alpha\beta}^* \mathbf{B}_{\beta}^* \times \mathbf{B}_3^* + K_{\alpha 3}^* \mathbf{B}_3^*) \times \mathbf{B}_i^* \end{aligned} \quad (58)$$

where the transverse shear strains are $\gamma = [2\gamma_{13} \quad 2\gamma_{23}]^T$. Since \mathbf{B}_i^* is uniquely determined by \mathbf{B}_i and γ , one can derive the following kinematic identity between the strains measures \mathcal{R} of Reissner–Mindlin plate and \mathcal{E} [29]:

$$\mathcal{E} = \mathcal{R} - \mathcal{D}_{\alpha} \gamma_{,\alpha} \quad (59)$$

where

$$\begin{aligned} \mathcal{D}_1 &= \begin{bmatrix} 0 & 0 & 0 & 1 & 0 & 0 \\ 0 & 0 & 0 & 0 & 1 & 0 \end{bmatrix}^T \\ \mathcal{D}_2 &= \begin{bmatrix} 0 & 0 & 0 & 0 & 1 & 0 \\ 0 & 0 & 0 & 0 & 0 & 1 \end{bmatrix}^T \end{aligned} \quad (60)$$

$$\mathcal{R} = [\varepsilon_{11}^* \quad 2\varepsilon_{12}^* \quad \varepsilon_{22}^* \quad K_{11}^* \quad K_{12}^* + K_{21}^* \quad K_{22}^*]^T$$

Now one can express the strain energy asymptotically correct to the second order in terms of strains of the Reissner–Mindlin model as

$$\begin{aligned} 2\Pi_1 &= \mathcal{R}^T A \mathcal{R} - 2\mathcal{R}^T A \mathcal{D}_1 \gamma_{,1} - 2\mathcal{R}^T A \mathcal{D}_2 \gamma_{,2} + \mathcal{R}_{,1}^T B \mathcal{R}_{,1} \\ &\quad + 2\mathcal{R}_{,1}^T C \mathcal{R}_{,2} + \mathcal{R}_{,2}^T D \mathcal{R}_{,2} - 2\mathcal{R}^T F \end{aligned} \quad (61)$$

The generalized Reissner–Mindlin model is of the form

$$2\Pi_{\mathcal{R}} = \mathcal{R}^T A \mathcal{R} + \gamma^T G_{\gamma} - 2\mathcal{R}^T F_{\mathcal{R}} - 2\gamma^T F_{\gamma} \quad (62)$$

To find an equivalent Reissner–Mindlin model Eq. (62) for Eq. (61), one has to eliminate all partial derivatives of the strain. Here, equilibrium equations are used to achieve this purpose. From the two equilibrium equations relating with the equilibrium of bending moments [30], one can obtain the following formula:

$$G_{\gamma} - F_{\gamma} = D_{\alpha}^T A \mathcal{R}_{,\alpha} + \begin{Bmatrix} m_1 \\ m_2 \end{Bmatrix} \quad (63)$$

where $F_{\mathcal{R},\alpha}$ is dropped because they are high-order terms. Substituting Eq. (63) into Eq. (61), one can show that $F_{\mathcal{R}} = F$ and $F_{\gamma} = 0$. Finally, one can rewrite Eq. (61) as

$$2\Pi_1 = \mathcal{R}^T A \mathcal{R} + \gamma^T G_{\gamma} - 2\mathcal{R}^T F + U^* \quad (64)$$

where

$$U^* = \mathcal{R}_{,1}^T \bar{B} \mathcal{R}_{,1} + 2\mathcal{R}_{,1}^T \bar{C} \mathcal{R}_{,2} + \mathcal{R}_{,2}^T \bar{D} \mathcal{R}_{,2} \quad (65)$$

and

$$\begin{aligned} \bar{B} &= B + A \mathcal{D}_1 G^{-1} \mathcal{D}_1^T A & \bar{C} &= C + A \mathcal{D}_1 G^{-1} \mathcal{D}_2^T A \\ \bar{D} &= D + A \mathcal{D}_2 G^{-1} \mathcal{D}_2^T A \end{aligned} \quad (66)$$

If we can drive U^* to be zero for any \mathcal{R} , then we have found an asymptotically correct Reissner–Mindlin plate model. For general anisotropic plates, this term will not be zero, but we can minimize the error to obtain a Reissner–Mindlin model being as asymptotically correct as possible. The accuracy of the Reissner–Mindlin model depends on how close to zero one can drive this term. In other words, one needs to seek an optimal set of the 27 unknowns (three unknowns for G and 24 unknowns for L_{α}) so that the value of the quadratic form in Eq. (65) is as close to zero as possible for arbitrary generalized strain measures. We let the distinct 78 terms in the symmetric 12×12 coefficient matrix equal to zeros to formulate 78 equations. It is a linear system with 27 unknowns. Then we use a least-squares technique to solve the overdetermined system for the constants. Mathematically, the overdetermined system (78 equations with 27 unknowns, indicated by $MX = b$) may be singular for some material properties. For example, the rank of $M^T M$ is only 26 for single-layer isotropic and orthotropic plates. In this situation, singular value decomposing technique can be applied to solve this least-squares

problem. Moreover, for an accurate estimation of the transverse shear matrix, a nondimensional scheme is used to guarantee that each of the 78 equations has the same physical unit.

From the asymptotic point of view, by driving U^* to zero, we obtain the best Reissner–Mindlin model, which will be used for 2-D plate analysis:

$$2\Pi_{\mathcal{R}} = \mathcal{R}^T A \mathcal{R} + \gamma^T G_{\gamma} - 2\mathcal{R}^T F \quad (67)$$

where A , G , and F capture the necessary material and geometric information obtained from the dimensional-reduction process. It is worthy to emphasize that although the 2-D constitutive model is constructed in a way dramatically different from traditional Reissner–Mindlin models, the plate analysis remains the same, with no changes in the governing equations and boundary conditions except that the strain measures are now defined using Eqs. (58).

V. Recovery Three-Dimensional Fields

Thus far, we have obtained a generalized Reissner–Mindlin model based on the asymptotically correct second-order energy for FGM plates. This model can be used for various analyses of FGM plates, spanning from static, dynamic, and buckling to aeroelastic analyses. In many applications, however, the capability of predicting accurate 2-D displacement fields of FGM plates is not sufficient. Ultimately, the fidelity of a reduced-order model should be evaluated based on how well it can predict the 3-D displacement/strain/stress fields for the original 3-D problem. Therefore, it is necessary to provide recovery relations to express the 3-D displacement, strain, and stress fields in terms of 2-D quantities and x_3 .

Using Eqs. (2), (4), and (5), one can recover the 3-D displacement field through the first order as

$$U_i = u_i + x_3(C_{3i} - \delta_{3i}) + C_{ji}w_j \quad (68)$$

where $w_{\alpha} = v_{\alpha}$ and $w_3 = C_{\perp}\mathcal{E}$. From Eq. (12), the 3-D strain field can be recovered up to the first order as

$$\Gamma_e = \epsilon + x_3\kappa, \quad 2\Gamma_s = v_{\parallel}^{\prime} + e_{\alpha}C_{\perp}\mathcal{E}_{,\alpha}, \quad \Gamma_t = C_{\perp}'\mathcal{E} \quad (69)$$

Consequently, 3-D stresses σ_{ij} can be obtained by applying the 3-D constitutive relations. Since we have obtained an optimal estimation of the shear stiffness matrix G , the recovered 3-D results up to the first order are better than CLT and FSDT. However, the transverse normal stress σ_{33} is a second-order quantity and cannot be estimated within the first-order approximation. Despite that it is usually much smaller than other stress components, σ_{33} is critical for predicting some structural failure mechanisms such as delamination. To obtain a reasonable recovery for the transverse normal stress, VAM procedure is applied once more to find the warping functions of second-order accuracy. Similarly, we perturb the warping functions as

$$w_{\parallel} = v_{\parallel} + y_{\parallel} + o\left(\left(\frac{h}{l}\right)^2 \eta\right), \quad w_3 = C_{\perp}\mathcal{E} + y_3 + o\left(\left(\frac{h}{l}\right)^2 \eta\right) \quad (70)$$

where y_{\parallel} and y_3 are the second-order warping functions. It can be shown that the in-plane components y_{\parallel} vanish and the equations governing y_3 are

$$\begin{aligned} (C_t^{(k)}y_3^{(k)} + C_{et}^{(k)T}I_{\alpha}v_{\parallel,\alpha}^{(k)})' + e_{\beta}^T C_s^{(k)}(v_{\parallel}^{(k)} + e_{\alpha}C_{\perp}^{(k)}\mathcal{E}_{,\alpha})_{,\beta} + \phi_3 &= \Lambda_3 \\ (C_t y_3' + C_{et}^T I_{\alpha} v_{\parallel,\alpha})^+ &= \tau_3, \quad (C_t y_3' + C_{et}^T I_{\alpha} v_{\parallel,\alpha})^- = -\beta_3 \\ [y_3] &= 0 \quad [C_t y_3' + C_{et}^T I_{\alpha} v_{\parallel,\alpha}] = 0, \quad \text{on } \Omega_i \end{aligned} \quad (71)$$

where Λ_3 is the Lagrange multiplier to enforce the constraint $\langle y_3 \rangle = 0$. The Euler–Lagrange equation and the intersurface continuity equation (71) can be expressed as

$$C_t^{(k)}y_3^{(k)} + C_{et}^{(k)T}I_{\alpha}v_{\parallel,\alpha}^{(k)} = E_{\alpha\beta}^{(k)}\mathcal{E}_{,\alpha\beta} + S^{(k)} + \Lambda_3 x_3 + \text{const}_{y_3}^{(k)}, \quad k = 1, 2, 3, \dots, N \quad (72)$$

$$\text{const}_{y_3}^{(k+1)} - \text{const}_{y_3}^{(k)} = E_{\alpha\beta}^{(k)}\mathcal{E}_{,\alpha\beta}(z_{k+1}) + S^{(k)}(z_{k+1}) \quad (73)$$

with

$$E_{\alpha\beta}^{(k)}(x_3) = - \int_{z_k}^{x_3} (e_{\alpha}^T D_{\beta}^{*(k)} + C_{s_{\alpha\beta}}^{(k)} C_{\perp}^{(k)}) dz \quad (74)$$

$$S^{(k)}(x_3) = - \int_{z_k}^{x_3} (e_{\alpha}^T g_{\alpha}^{*(k)} + \phi_3^{(k)}) dz \quad (75)$$

The Lagrange multiplier Λ_3 and the solution of y_3 are given by

$$\Lambda_3 = \frac{1}{h}(\tau_3 + \beta_3 - \langle E'_{\alpha\beta} \rangle \mathcal{E}_{,\alpha\beta} - \langle S' \rangle) \quad (76)$$

$$y_3^{(k)} = \bar{E}_{,\alpha\beta}^{(k)} \mathcal{E}_{,\alpha\beta} + \bar{S}^{(k)} \quad (77)$$

with

$$\bar{E}_{\alpha\beta}^{(k)} = C_t^{(k)-1} E_{\alpha\beta}^{(k)*}, \quad \langle \bar{E}_{\alpha\beta}^{(k)} \rangle = 0, \quad \bar{S}^{(k)} = C_t^{(k)-1} S^{(k)*}, \quad \langle \bar{S} \rangle = 0$$

where $E_{\alpha\beta}^{(k)*}$ and $S^{(k)*}$ can be obtained from Eqs. (72), (73), and (76) as well as the interlaminar continuous conditions in the last equation of Eq. (71).

Although y_3 can help us obtain an energy expression asymptotically corrected up to the order of $(h/l)^4 \eta^2$, such an energy expression is too complex for practical use. We will still use the Reissner–Mindlin model to carry out the 2-D plate analysis and use y_3 for the second-order prediction of the 3-D displacement/strain/stress field. As will be shown later, this approach achieves excellent predictions even though only the Reissner–Mindlin plate model is used for the 2-D plate analysis.

Finally, we can recover the 3-D displacement field up to the second order as

$$U_i = u_i + x_3(C_{3i} - \delta_{3i}) + C_{ji}w_j + \delta_{3i}C_{3i}y_3 \quad (78)$$

and the strains up to the second order as

$$\Gamma_e = \epsilon + x_3\kappa + I_{\alpha}v_{\parallel,\alpha}, \quad 2\Gamma_s = v_{\parallel}^{\prime} + e_{\alpha}C_{\perp}\mathcal{E}_{,\alpha}, \quad \Gamma_t = C_{\perp}'\mathcal{E} + y_3' \quad (79)$$

Finally, we can recover the 3-D stress field up to the second order as

$$\begin{aligned} [\sigma_{11} \quad \sigma_{12} \quad \sigma_{22}]^T &= C_{\parallel}(\epsilon + x_3\kappa) + C_{et}y_3' + C_e I_{\alpha}v_{\parallel,\alpha} \\ [\sigma_{13} \quad \sigma_{23}]^T &= C_s(v_{\parallel}^{\prime} + e_{\alpha}C_{\perp}\mathcal{E}_{,\alpha}), \quad \sigma_{33} = C_{et}^T I_{\alpha}v_{\parallel,\alpha} + C_t y_3' \end{aligned} \quad (80)$$

VI. Validation Examples

We have derived a general formulation to treat multilayer plates made of functionally graded materials with properties as functions of x_3 . In the following, we will use several examples to demonstrate the performance of the present theory.

The first example is a single-layer, simply supported, square, functionally graded plate. The width of the plate is denoted as a . The top surface of the FGM plate is ceramic rich and the bottom surface is metal-rich. The region between the two surfaces is made of the mixture of ceramic-metal materials with continually varying of the volume fractions of the ceramic and metal. The volume fraction of the ceramics V_c is assumed to vary according to a power law as

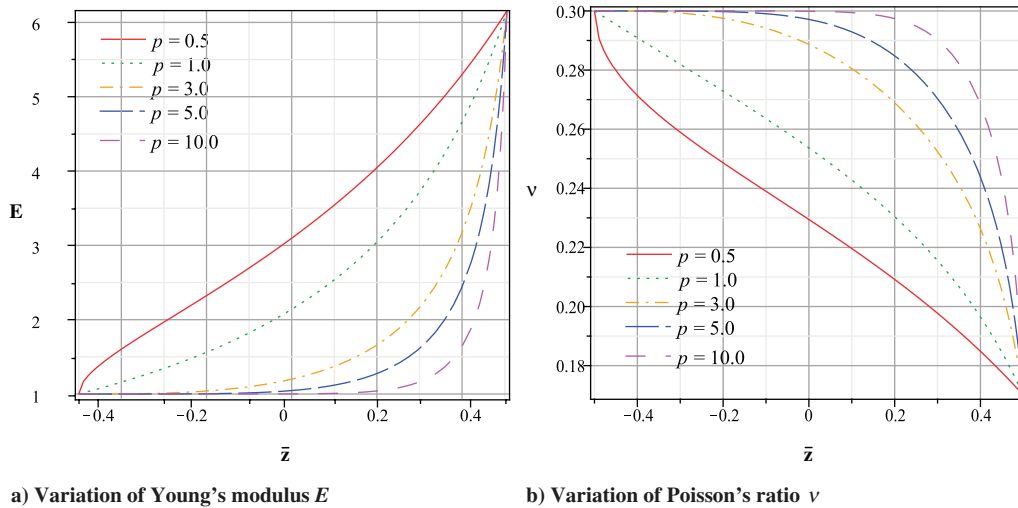


Fig. 2 Through-the-thickness variation of effective Young's modulus E and Poisson's ratio ν estimated by Mori–Tanaka scheme for different values of p .

$$V_c = V_c^- + (V_c^+ - V_c^-) \left(\frac{1}{2} + \frac{x_3}{h} \right)^p, \quad p \geq 0$$

where V_c^+ and V_c^- are the volume fractions of the ceramic on the top and the bottom surfaces, respectively; p is the volume fraction index, and h the thickness of the plate. The effective elastic moduli of the functionally graded metal-ceramic material are estimated by the Mori–Tanaka scheme as

$$\begin{cases} \frac{K^* - K_m}{K_c - K_m} = \frac{V_c}{1 + (1 - V_c) \frac{K_c - K_m}{K_m + \frac{2}{3}\mu_m}} \\ \frac{\mu^* - \mu_m}{\mu_c - \mu_m} = \frac{V_c}{1 + (1 - V_c) \frac{\mu_c - \mu_m}{\mu_m + s_1}} \end{cases} \quad (81)$$

where $s_1 = \mu_m(9K_m + 8\mu_m)/(6(K_m + 2\mu_m))$, K_m and μ_m represent the bulk and shear modulus of the metal, and K_c and μ_c represent the bulk and shear modulus of the ceramic material [9,16]. Young's

modulus $E(x_3)$ and Poisson's ratio $\nu(x_3)$ are related to effective bulk and shear moduli by

$$K^*(x_3) = \frac{E(x_3)}{3[1 - 2\nu(x_3)]}, \quad \mu^*(x_3) = \frac{E(x_3)}{2[1 + \nu(x_3)]} \quad (82)$$

For the purpose of illustration, we choose the properties of the constituent materials as $E_m = 70$ GPa and $\nu_m = 0.3$ for Al, and $E_c = 427$ GPa and $\nu_c = 0.17$ for SiC. Figure 2 plots through-the-thickness variation of effective Young's modulus and Poisson's ratio for various material index p .

The FGM plate is subjected to a sinusoidally distributed pressure on the top surface, described by

$$\tau_3(x_1, x_2) = q_0 \sin(\pi x_1/a) \sin(\pi x_2/a)$$

There is no body force and the bottom surface is traction-free. To facilitate our comparison, the physical quantities are nondimensionalized by the following relations:

Table 1 Comparison of displacements and stresses at specific locations with 3-D elasticity solutions for Al/SiC functionally graded plates at $V_c^- = 0$, $V_c^+ = 0.5$, and $p = 2$

Variable	$a/h = 5$		$a/h = 10$		$a/h = 40$	
	Exact	Present	Exact	Present	Exact	Present
$\bar{U}_1(0, a/2, h/2)$	-2.9129	-2.9124	-2.8997	-2.8987	-2.8984	-2.8983
$\bar{U}_3(0, a/2, 0)$	2.5748	2.5716	2.2266	2.2256	2.1163	2.1163
$\bar{U}_3(0, a/2, h/2)$	2.5559	2.5524	2.2148	2.2139	2.1155	2.1154
$\bar{\sigma}_{11}(a/2, a/2, h/2)$	2.7562	2.7558	2.6424	2.6415	2.6093	2.6092
$\bar{\sigma}_{12}(0, 0, h/2)$	-1.5600	-1.5597	-1.5529	-1.5524	-1.5522	-1.5521
$\bar{\sigma}_{13}(0, a/2, 0)$	2.3100	2.2749	2.3239	2.3150	2.3281	2.3276
$\bar{\sigma}_{33}(a/2, a/2, h/4)$	0.8100	0.8117	0.8123	0.8127	0.8129	0.8129

Table 2 Comparison of displacements and stresses at specific locations with 3-D elasticity solutions for Al/SiC functionally graded plates at $V_c^- = 0$, $p = 2$, and $a/h = 5$

Variable	$V_c^+ = 0.2$		$V_c^+ = 0.6$		$V_c^+ = 1.0$	
	Exact	Present	Exact	Present	Exact	Present
$\bar{U}_1(0, a/2, h/2)$	-3.6982	-3.6966	-2.6708	-2.6697	-1.7421	-1.7359
$\bar{U}_3(0, a/2, 0)$	3.0254	3.0215	2.4326	2.4293	1.8699	1.8634
$\bar{U}_3(0, a/2, h/2)$	2.9852	2.9808	2.4196	2.4160	1.8767	1.8702
$\bar{\sigma}_{11}(a/2, a/2, h/2)$	2.3285	2.3273	2.9359	2.9347	4.1042	4.0899
$\bar{\sigma}_{12}(0, 0, h/2)$	-1.2163	-1.2158	-1.7106	-1.7099	-2.8534	-2.8433
$\bar{\sigma}_{13}(0, a/2, 0)$	2.3516	2.3065	2.2918	2.2604	2.1805	2.1683
$\bar{\sigma}_{33}(a/2, a/2, h/4)$	0.8300	0.8284	0.8024	0.8047	0.7623	0.7675

$$\bar{U}_\alpha = \frac{100Eh^2U_\alpha}{q_0a^3}, \quad \bar{U}_3 = \frac{100Eh^3U_3}{q_0a^4}, \quad \bar{\sigma}_{\alpha\beta} = \frac{10h^2\sigma_{\alpha\beta}}{q_0a^2}$$

$$\bar{\sigma}_{\alpha 3} = \frac{10h\sigma_{\alpha 3}}{q_0a}, \quad \bar{\sigma}_{33} = \frac{\sigma_{33}}{q_0}$$

Tables 1 and 2 provide a detailed comparison of displacement and stress components with exact 3-D solution [9] at various critical locations of the plate. Results in Table 1 ($V_c^- = 0, V_c^+ = 0.5,$ and $p = 2$) indicate the effect of a/h on displacement and stress components. It shows an excellent match between the present plate

theory and the 3-D exact solution. The maximum percentage error occurs for σ_{13} (1.5%) when $a/h = 5,$ with the percentage errors for other components being less than 0.21%. As expected, the relative errors for displacement and stress components decrease as a/h increases. For example, when $a/h = 10,$ the maximum percentage error still occurs for σ_{13} with a value of 0.38% and the relative errors for other components being less than 0.04%. The effect of volume fraction of the ceramic constituent for a thick functionally graded plate ($V_c^- = 0, p = 2,$ and $a/h = 5$) is provided in Table 2. Again, all stress and displacement results match very well with the exact solutions. The maximum percentage error takes the value of

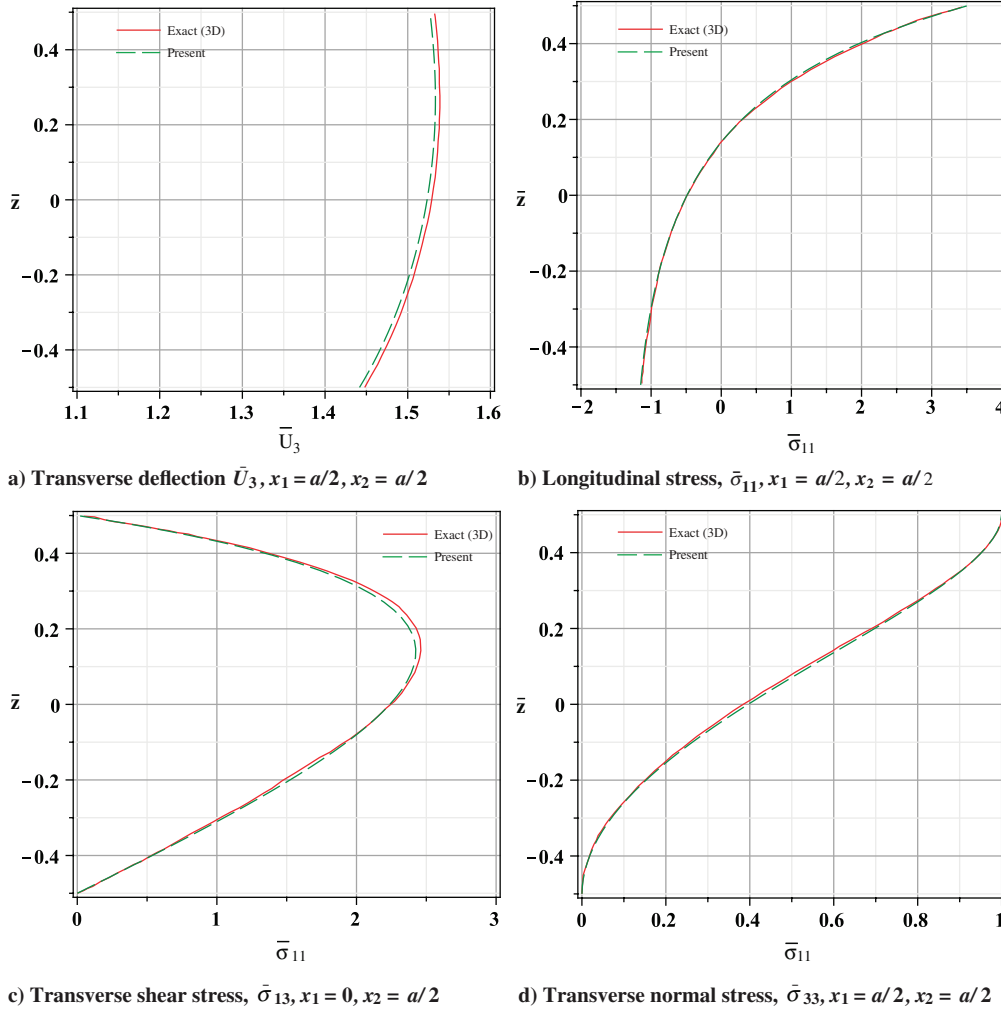


Fig. 3 Nondimensional transverse deflection, longitudinal stress, transverse shear stress, transverse normal stress distributions along the thickness direction for a Ai/Sic FGM square plate under sinusoidal pressure on the top surface; $V_c^- = 0, V_c^+ = 1.0, p = 1,$ and $a/h = 5.$

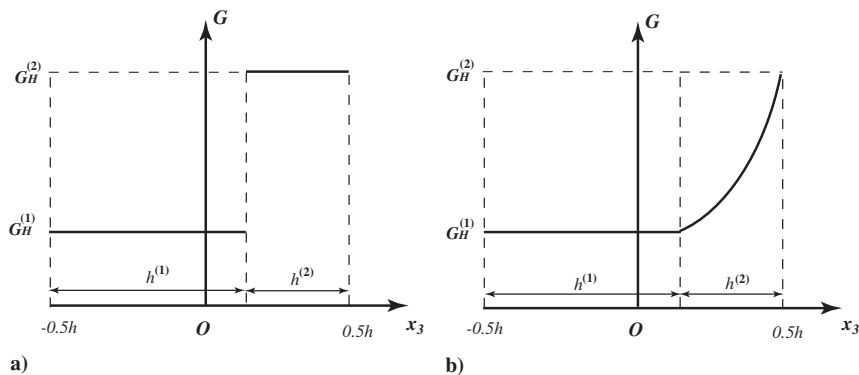


Fig. 4 Through-the-thickness variation of shear moduli G in two coating/substrate systems: a) system H and b) system $F.$

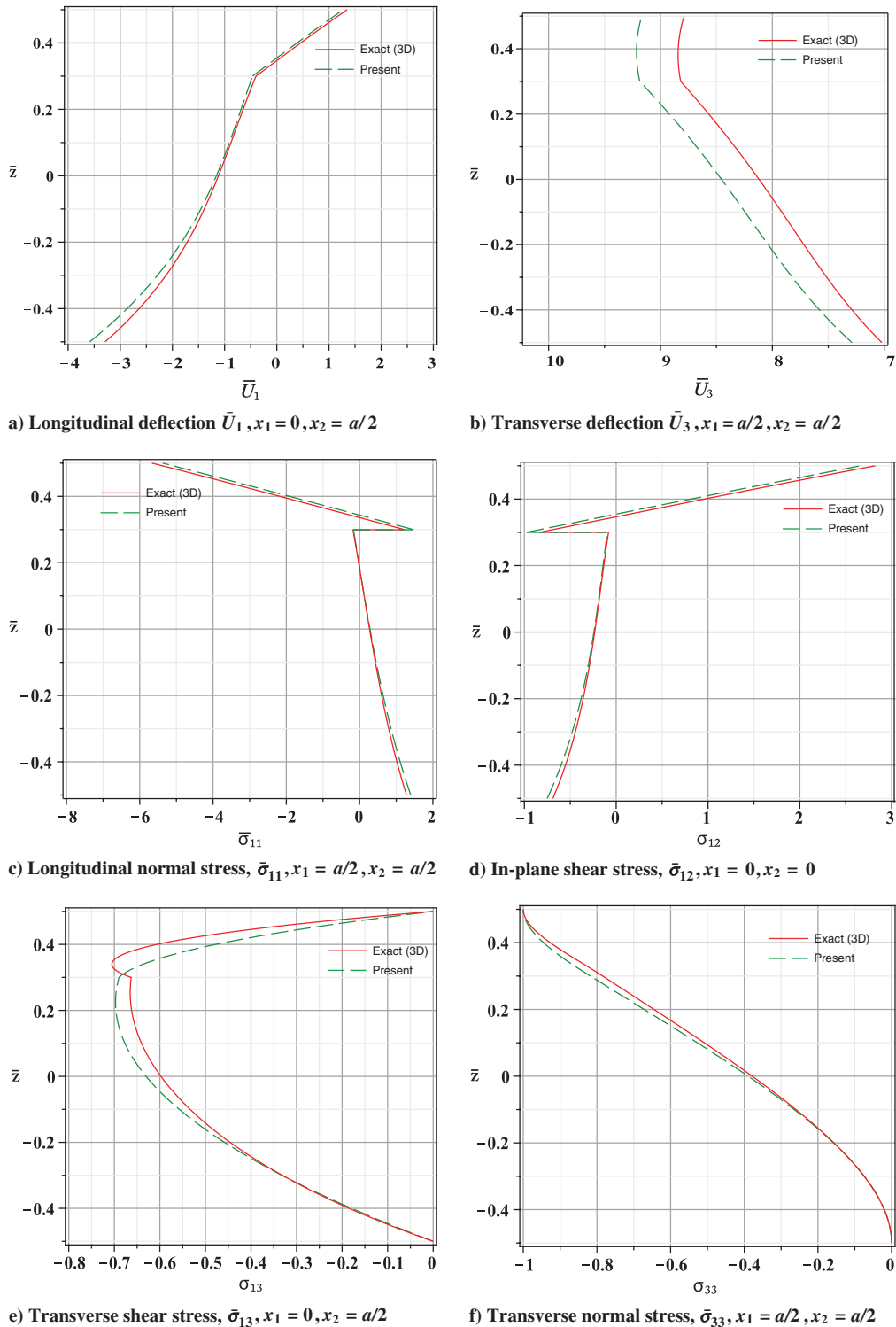


Fig. 5 Through-the-thickness variation of nondimensional displacements and stresses for a thick two-layer homogeneous coating/substrate system (system H) under sinusoidal pressure on the top surface ($a/h = b/h = 3$).

$\sigma_{13} = 1.9\%$, $\sigma_{13} = 1.4\%$, and $\sigma_{33} = 1.67\%$ for $V_c^+ = 0.2$, $V_c^+ = 0.6$, and $V_c^+ = 1.0$, respectively, whereas the relative errors for other components are less than 0.14, 0.29, and 0.55% corresponding to these three cases. From this example, one can also observe that the present model, although based on asymptotic analysis of the small parameter h/l ($l = a$ for this example), can provide fairly good prediction for not so small parameters such as for this case $h/l = 0.2$. However, because no further data of the 3-D solutions is available from the reference, the accuracy of present plate model for thicker plates cannot be estimated. Nevertheless, the present 2-D plate model can be shown to achieve a high accuracy even for fairly large h/l . For

example, in [25], we analyzed the cylindrical bending of an isotropic homogeneous plate. For an extremely thick plate with $h/l = 0.5$, the maximum relative error among all the 3-D fields less than 6%, in comparison with the 3-D exact solution.

Further comparisons are also made for another FGM plate with $V_c^- = 0$, $V_c^+ = 1$, $p = 1$, $a/h = 5$. The results are plotted in Fig. 3, in which $\bar{z} = x_3/h$. Both magnitude and trend match very well with the exact solution, which again demonstrates that the present plate model can be used to accurately predict FGM plates.

The second example is two double-layer coating/substrate systems, as discussed in [4,5], including a homogeneous substrate

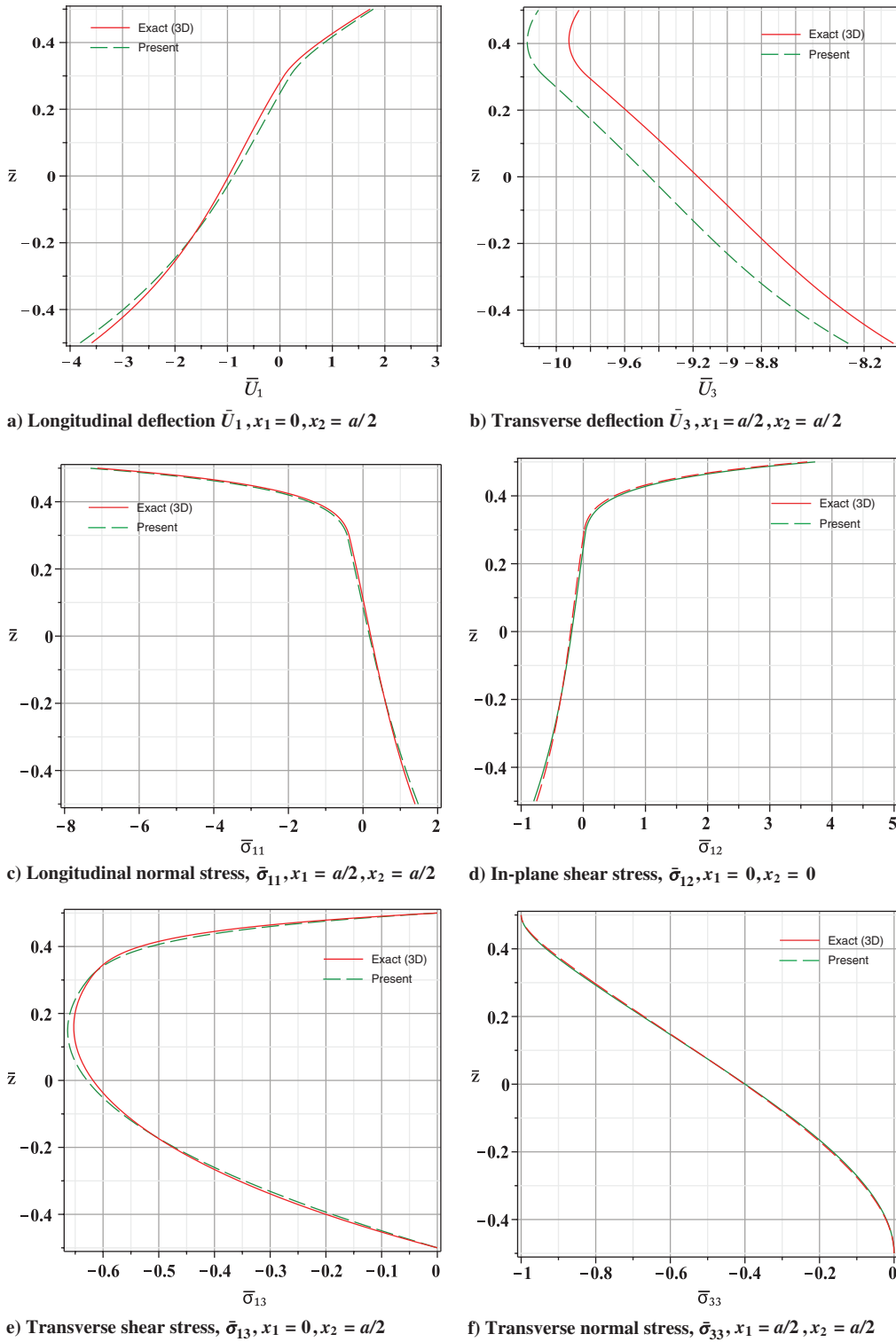


Fig. 6 Through-the-thickness variation of nondimensional displacements and stresses for a thick two-layer functionally graded coating/substrate system (system F) under sinusoidal pressure on the top surface ($a/h = b/h = 3$).

with a thin homogeneous coating (system H) and a homogeneous substrate with a thin functionally graded coating (system F). In both systems, Poisson's ratios for the substrate and the coating are assumed to be constants and equal, i.e., $\nu_H^{(1)} = \nu_H^{(2)} = \nu_F^{(1)} = \nu_F^{(2)} = 0.3$. The shear modulus of the substrate and the coating for system H takes the value of $G_H^{(1)}, G_H^{(2)}$, respectively, and for system F , the shear modulus of the substrate and the coating takes the form of

$$G_F^{(1)} = G_H^{(1)}, \quad G_F^{(2)}(x_3) = \xi G_H^{(2)} e^{\theta(x_3/h - 1)}$$

where $\xi = G_H^{(2)}/G_H^{(1)}$ is the ratio of the stiffness on the top of the functionally graded coating to that of the homogeneous substrate; $\theta = h/h^{(2)} \ln \xi$ is the inhomogeneous parameter of the functionally graded coating; and $h^{(2)}$ is the coating thickness. The through-the-thickness variation of shear moduli G for two systems is shown in Fig. 4. In the present analysis, ξ and $h/h^{(2)}$ are chosen to be 10 and 5, respectively. The plate is assumed to be simply supported and subjected to the following boundary conditions:

$$x=0, a: \sigma_{11} = 0, \quad U_2 = U_3 = 0, \quad y=0, b: \sigma_{22} = 0, \quad U_1 = U_3 = 0$$

The top surface of the coating at $x_3 = h/2$ is subjected to a sinusoidally distributed pressure $[\tau_3 = -q_0 \sin(\pi x_1/a) \sin(\pi x_2/b)]$, and the bottom surface of the substrate is traction-free. Again, no body force is applied. The stress and displacement components are nondimensionalized as $\bar{\sigma}_{ij} = \sigma_{ij}/q_0$ and $\bar{U}_i = U_i G_H^{(2)}/(q_0 h)$. A general solution procedure for inhomogeneous isotropic media free of body forces is developed by Plevako [31] and was applied to simplify supported multilayer functionally graded plates [4,5]. Because of some typos existing in the formulas in [4], the authors rederived the 3-D exact solutions for the multilayer functionally graded plate. Moreover, unlike in [4,5], in which solutions for homogeneous plate are approximated by using a small inhomogeneous parameter θ , exact solutions for homogeneous plate are derived and used in the results presented here.

Figure 5 depicts the through-thickness variation of nondimensional in-plane displacement \bar{U}_1 , transverse displacement \bar{U}_3 , longitudinal normal stress $\bar{\sigma}_{11}$, in-plane shear stress $\bar{\sigma}_{12}$, transverse shear stress $\bar{\sigma}_{13}$, and transverse normal stress $\bar{\sigma}_{33}$ for a thick ($a/h = b/h = 3$) homogeneous coating/substrate system (system H). It can be observed that all in-plane stress and displacement components, \bar{U}_1 , $\bar{\sigma}_{11}$, and $\bar{\sigma}_{12}$ and transverse normal stress $\bar{\sigma}_{33}$ match very well with the 3-D exact solution. Because of the discontinuity of the shear modulus G for the homogeneous coating and homogeneous substrate, there exist some jumps for in-plane normal $\bar{\sigma}_{11}$ stress and shear stress $\bar{\sigma}_{12}$ at the interface. It seems that there exists a constant shift (about 5% of the maximum value) between the results of the present model and the 3-D solution for the transverse displacement \bar{U}_3 . This may be attributed to that our plate model is reduced from the original 3-D model and some information that cannot be captured by a 2-D model are lost during the dimensional-reduction process. Further investigation shows that there are some discrepancies near the interface of the coating/substrate between the present theory and the 3-D solution for the transverse shear stress $\bar{\sigma}_{13}$: the 3-D solution presents a sharp change of $\bar{\sigma}_{13}$ inside the coating layer, whereas our model has a more smooth transition. Nevertheless, both results show similar maximum value for $\bar{\sigma}_{13}$.

The through-thickness variations of various displacement and stress components for a thick ($a/h = b/h = 3$) double-layer functionally graded coating/substrate system (system F) are plotted in Fig. 6. It can be observed from this figure that all displacement and stress components except for \bar{U}_3 match well with the exact 3-D solutions. Similar constant shift can be observed between the present model and the 3-D exact solution. It is important to note that by adopting functionally graded coating the shear moduli G is now continuous at the interface, the in-plane stress components such as $\bar{\sigma}_{11}$ and $\bar{\sigma}_{12}$ therefore become smooth throughout of the total thickness of the F system. In addition, no sharp peak appears for transverse shear stress $\bar{\sigma}_{13}$. Results presented in Fig. 6 clearly show that using functionally graded coating instead of the homogeneous one will eliminate the mismatch of interface stress components to reduce the risk of cracking and rebounding of the coating.

VII. Conclusions

An efficient high-fidelity plate model for multilayer functionally graded plate has been developed using the variational-asymptotic method (VAM). By taking advantage of the small parameter h/l , VAM is used to systematically reduce the original nonlinear 3-D model to a series of 2-D models in terms of the small parameter. No a priori assumptions have been adopted during the derivation. The theory is applicable to functionally graded plates with material properties either being constant or changing continuously in each layer. Although the resulting plate theory is as simple as a single-layer FSDT, the recovered 3-D displacement, strain, and stress results have excellent accuracy in comparison with the 3-D elasticity. Moreover, the present model is valid for large displacements and global rotations and can capture all the geometric nonlinearity of a plate when the strains are small. The present paper has built on the second author's previous work [19,21] with the following new contributions:

- 1) The present work has the capability of analyzing multilayer functionally graded plate with material properties as functions of transverse locations or constant, whereas in previous work, these properties are treated as constants for each layer.
- 2) Interface continuity conditions are explicitly derived and solved to obtain the multilayer solutions.
- 3) Simplifications have been made in deriving B , C , and D matrices.
- 4) Explicit analytical solutions for the second-order approximation of warping functions have been provided.
- 5) A nondimensional scheme has been applied on solving the least-squares problem resulting in a more reliable estimation of the transverse shear stiffness matrix.

Acknowledgments

The present work is supported in part by the U.S. Air Force Office of Scientific Research under grant FA9550-08-1-0405. The Program Managers are Victor Giurgiutiu and David Stargel. The views and conclusions contained herein are those of the authors and should not be interpreted as necessarily representing the official policies or endorsement, either expressed or implied, of the funding agency.

References

- [1] Müller, E., Drašar, Č., Schilz, J., and Kaysser, W. A., "Functionally Graded Materials for Sensor and Energy Applications," *Materials Science and Engineering A*, Vol. 362, Nos. 1–2, 2003, pp. 17–39. doi:10.1016/S0921-5093(03)00581-1
- [2] Mishnaevsky, L. L., Jr., "Functionally Gradient Metal Matrix Composites: Numerical Analysis of the Microstructure-Strength Relationships," *Composites Science and Technology*, Vol. 66, Nos. 11–12, 2006, pp. 1873–1887. doi:10.1016/j.compscitech.2005.09.003
- [3] Shaw, L. L., "Thermal Residual Stresses in Plates and Coatings Composed of Multi-Layered and Functionally Graded Materials," *Composites, Part B*, Vol. 29, No. 3, 1998, pp. 199–210. doi:10.1016/S1359-8368(97)00029-2
- [4] Kashtalyan, M., and Menshykova, M., "Three-Dimensional Elastic Deformation of a Functionally Graded Coating/Substrate System," *International Journal of Solids and Structures*, Vol. 44, No. 16, 2007, pp. 5272–5288. doi:10.1016/j.ijsolstr.2006.12.035
- [5] Kashtalyan, M., and Menshykova, M., "Three-Dimensional Analysis of a Functionally Graded Coating/Substrate System of Finite Thickness," *Philosophical Transactions of the Royal Society of London, Series A: Mathematical and Physical Sciences*, Vol. 366, No. 1871, 2008, pp. 1821–1826. doi:10.1098/rsta.2007.2194
- [6] Das, M., Barut, A., Madenci, E., and Ambur, D. R., "A Triangular Plate Element for Thermo-Elastic Analysis of Sandwich Panels with a Functionally Graded Core," *International Journal for Numerical Methods in Engineering*, Vol. 68, No. 9, 2006, pp. 940–966. doi:10.1002/nme.1724
- [7] Shang, F., Wang, Z., and Li, Z., "Analysis of Thermally Induced Cylindrical Flexure of Laminated Plates with Piezoelectric Layers," *Composites, Part B*, Vol. 28B, No. 3, 1997, pp. 185–193.
- [8] Pan, E., and Heyliger, P. R., "Exact Solution for Magneto-Electro-Elastic Laminates in Cylindrical Bending," *International Journal of Solids and Structures*, Vol. 40, No. 24, 2003, pp. 6859–6876. doi:10.1016/j.ijsolstr.2003.08.003
- [9] Vel, S. S., and Batra, R. C., "Exact Solution for Thermoelastic Deformations of Functionally Graded Thick Rectangular Plates," *AIAA Journal*, Vol. 40, No. 7, 2002, pp. 1421–1433. doi:10.2514/2.1805
- [10] Altay, G., and Dökmeci, M. C., "Variational Principles and Vibrations of a Functionally Graded Plate," *Computers and Structures*, Vol. 83, Nos. 15–16, 2005, pp. 1340–1354. doi:10.1016/j.compstruc.2004.09.017
- [11] Liew, K. M., He, X. Q., Ng, T. Y., and Sivashanker, S., "Active Control of FGM Plates Subjected to a Temperature Gradient: Modelling via Finite Element Method Based on FSDT," *International Journal for Numerical Methods in Engineering*, Vol. 52, No. 11, 2001, pp. 1253–1271. doi:10.1002/nme.252
- [12] Ma, L. S., and Wang, T. J., "Relationships Between Axisymmetric Bending and Buckling Solutions of FGM Circular Plates Based on

- Third-Order Plate Theory and Classical Plate Theory," *International Journal of Solids and Structures*, Vol. 41, No. 1, 2004, pp. 85–101.
doi:10.1016/j.ijsolstr.2003.09.008
- [13] Bian, Z. G., Chen, W. Q., Lim, C. W., and Zhang, N., "Analytical Solutions for Single- and Multi-Span Functionally Graded Plates in Cylindrical Bending," *International Journal of Solids and Structures*, Vol. 42, Nos. 24–25, 2005, pp. 6433–6456.
doi:10.1016/j.ijsolstr.2005.04.032
- [14] Soldatos, K. P., and Watson, P., "A Method for Improving the Stress Analysis Performance of One-And Two-Dimensional Theories for Laminated Composites," *Acta Mechanica*, Vol. 123, Nos. 1–4, 1997, pp. 163–186.
doi:10.1007/BF01178408
- [15] Soldatos, K. P., and Watson, P., "Accurate Stress Analysis of Laminated Plates Combining a Two-Dimensional Theory with the Exact Three-Dimensional Solution for Simply Supported Edges," *Mathematics and Mechanics of Solids*, Vol. 2, No. 4, 1997, pp. 459–489.
doi:10.1177/108128659700200405
- [16] Gilhooley, D. F., Batra, R. C., Xiao, J. R., McCarthy, M. A., and Gillespie, J. W., Jr., "Analysis of Thick Functionally Graded Plates by Using Higher-Order Shear and Normal Deformable Plate Theory and MLPG Method with Radial Basis Functions," *Composite Structures*, Vol. 80, No. 4, 2007, pp. 539–552.
doi:10.1016/j.compstruct.2006.07.007
- [17] Zhen, W., and Chen, W., "A Higher-Order Theory and Refined Three-Node Triangular Element For Functionally Graded Plates," *European Journal of Mechanics, A/Solids*, Vol. 25, 2006, pp. 447–463.
doi:10.1016/j.euromechsol.2005.09.009
- [18] Berdichevsky, V. L., "Variational-Asymptotic Method of Constructing a Theory of Shells," *Journal of Applied Mathematics and Mechanics*, Vol. 43, No. 4, 1979, pp. 711–736.
doi:10.1016/0021-8928(79)90157-6
- [19] Yu, W., Hodges, D. H., and Volovoi, V. V., "Asymptotic Construction of Reissner-Like Composite Plate Theory with Accurate Strain Recovery," *International Journal of Solids and Structures*, Vol. 39, No. 20, 2002, pp. 5185–5203.
doi:10.1016/S0020-7683(02)00410-9
- [20] Yu, W., and Hodges, D. H., "A Simple Thermopiezoelectric Model for Composite Plates with Accurate Stress Recovery," *Smart Materials and Structures*, Vol. 13, No. 4, 2004, pp. 926–938.
doi:10.1088/0964-1726/13/4/031
- [21] Yu, W., "Mathematical Construction of a Reissner–Mindlin Plate Theory for Composite Laminates," *International Journal of Solids and Structures*, Vol. 42, No. 26, 2005, pp. 6680–6699.
doi:10.1016/j.ijsolstr.2005.02.049
- [22] Chen, H., and Yu, W., "Postbuckling and Mode Jumping Analysis of Composite Laminates Using an Asymptotically Correct, Geometrically Non-Linear Theory," *International Journal of Non-Linear Mechanics*, Vol. 41, No. 10, 2006, pp. 1143–1160.
doi:10.1016/j.ijnonlinmec.2006.11.004
- [23] Liao, L., and Yu, W., "Asymptotical Construction of a Fully Coupled, Reissner–Mindlin Model for Piezoelectric Composite Plates," *Smart Materials and Structures*, Vol. 17, No. 1, 2008, Paper 015010.
doi:10.1088/0964-1726/17/01/015010
- [24] Liao, L., and Yu, W., "An Electromechanical Reissner-Mindlin Model for Laminated Piezoelectric Plates," *Composite Structures*, Vol. 88, No. 3, 2009, pp. 394–402.
doi:10.1016/j.compstruct.2008.04.017
- [25] Chen, H., and Yu, W., "Asymptotical Construction of an Efficient High-Fidelity Model For Functional Graded Plates," 50th AIAA/ASME/ASCE/AHS/ASC Structures, Structural Dynamics, and Materials Conference, AIAA, Paper 2009-2135, Palm Springs, CA, May 2009.
- [26] Danielson, D. A., and Hodges, D. H., "Nonlinear Beam Kinematics by Decomposition of the Rotation Tensor," *Journal of Applied Mechanics*, Vol. 54, No. 2, 1987, pp. 258–262.
doi:10.1115/1.3173004
- [27] Danielson, D. A., "Finite Rotation with Small Strain in Beams and Plates," *Proceedings of the 2nd Pan American Congress of Applied Mechanics*, Valparaiso, Chile, Jan. 1991.
- [28] Atilgan, A. R., Hodges, D. H., and Danielson, D. A., "A Geometrically Nonlinear Theory of Elastic Plates," *Journal of Applied Mechanics*, Vol. 60, No. 1, 1993, pp. 109–116.
doi:10.1115/1.2900732
- [29] Yu, W., "Variational Asymptotic Modeling of Composite Dimensionally Reducible Structures," Ph.D. Thesis, Aerospace Engineering, Georgia Inst. of Technology, Atlanta, May 2002.
- [30] Atilgan, A. R., and Hodges, D. H., "On the Strain Energy of Laminated Composite Plates," *International Journal of Solids and Structures*, Vol. 29, No. 20, 1992, pp. 2527–2543.
doi:10.1016/0020-7683(92)90007-G
- [31] Plevako, V. P., "On the Theory of Elasticity of Inhomogeneous Media," *Journal of Applied Mathematics and Mechanics*, Vol. 35, No. 5, 1971, pp. 806–813.
doi:10.1016/0021-8928(71)90078-5

A. Palazotto
Associate Editor